CHARACTERIZATION OF MICROINSTABILITIES IN HALL THRUSTER PLASMA: EXPERIMENTAL AND PIC CODE SIMULATION RESULTS, PHYSICAL INTERPRETATION AND IMPACT ON TRANSVERSE ELECTRON TRANSPORT

A. Lazurenko[*], V. Vial[*], A. Bouchoule[*], M.Prioul[**], J.C. Adam[***], A. Heron[***], G. Laval[***]
[*] GREMI, Université d'Orléans, BP 6744, 45067 Orléans, France
andre.bouchoule@univ-orleans.fr
[**] SNECMA, Villaroche Nord, B.P. n°93, F-77552 Moissy-Cramayel Cédex
mathieu.prioul@snecma.fr
[***] CPHT, Ecole Polytechnique, route de Saclay, 91128 Palaiseau, France
adam@cpht.polytechnique.fr, laval@cpht. polytechnique.fr

Paper IEPC-2003 – 0218 – Toulouse, France

Non-intrusive time- and spatially-resolved (in azimuthal direction) diagnostics has been developed for investigation of high frequency (HF) oscillations in Hall thrusters. There was discovered a low-frequency modulation of HF oscillations which correlates with low-frequency discharge current oscillations and have a relation with electron transport in these thrusters. HF oscillations were identified as azimuthal waves propagating with the velocity close to that one of electron drift, that is in agreement with earlier observations done by other diagnostics [1]. Observed HF oscillations have a definite, well shaped structure and there was suggested their source as fluctuations of electron number density. Possible correlation with total electric field variation in Hall thruster was revealed. Presented here the latest results of numerical study of plasma stability on the base of the 2D fully kinetic model show an existence of strong electric field oscillations which can reach 20% of the accelerating field. These oscillation are responsible for the "anomalous" axial electron transport. In order to understand the origin of this turbulence, we have studied the dispersion equation of electrostatic waves in a plasma at the presence of magnetic field. It was shown the possibility of appearance of oscillations with frequency ~1-10MHz with short growth times.

Introduction

Oscillations of different frequencies are observed in Hall effect thrusters. Carried out to the present moment theoretical and experimental studies allowed for classification of the oscillations and determination of the conditions of their appearance. From the all variety of oscillations, low- and middle-frequency ones (f<1MHz) are well documented in the literature, possible physical phenomena responsible for their appearance were revealed [1,2,3,4,5]. High frequency oscillations (HF) with f≥1-10MHz were studied relatively poor. Instabilities from this frequency band are the most likely associated with electron dynamics in these thrusters [6]. The latter is not well understood by now, and therefore investigation of the HF oscillations can give a better understanding of this subject.
One of the first studies concerning HF oscillations in Hall thrusters was performed by Esipchuk and Tilinin [1]. More recently, Choueiri presented results of the HF oscillations analysis. Experiments, previously conducted in our laboratory [7] with the use of the probe of electron drift current, revealed the correlation between microinstabilities f~5-10 MHz and macroscopic transport phenomena. Also, 2D simulations developed in France [8] prove the possibility of such correlation and suggest that these microinstabilities can be involved in enhanced axial electron transport. Nevertheless, the total picture of electron transport through the region of strong electric and magnetic fields is still unclear.
In the this paper the authors present the recent experimental results on HF oscillation investigation in SPT-100ML thruster with the use high frequency band antennas, results of 2D simulation on the base of developed PIC model and analysis of dispersion equation of waves in a plasma at the presence of magnetic field.

I. Experimental studies of microinstabilities

I.1 Inputs of the present studies

In the work of Esipchuk and Tilinin [1] there was presented a theoretical investigation of the oscillation processes in Hall effect thrusters. It was based on the two-fluid (electrons and ions) description without

collisions, under the assumption of weak plasma nonuniformity. Obtained dispersion equation allowed for prediction of different types of instabilities, longitudinal and azimuthal. The latter were predicted, in particular, in the form of azimuthal high frequency waves, which should be localized in the region of $\frac{d}{dx}\left(\frac{H}{n}\right)<0$, where H – magnetic field, n – plasma number density (at the condition of quasineutrality). Subsequent experiments of these authors, with the use of near-wall probes, discovered these waves in the region of the negative magnetic field gradient. The frequency of these waves was f~2-5 MHz. They were identified as electron drift waves because the direction of their propagation coincides with the direction of electron drift, and the velocity is close to that of electron drift. Earlier Morozov et al showed [9] that intentionally induced by electrostatic probes instabilities propagate on azimuth likely in the direction of electron drift. Choueiri in his analysis [4] predicts the HF azimuthal instabilities also in the region with positive gradient of magnetic field. But by now, there has not been done any observation on correlation of this type of instabilities and particle transport along the channel.

In our recent work [7] we observed a correlation of microinstabilities (f~5-10 MHz) with discharge current waveform. They were registered by the probe of electron drift current which is a wire loop inserted in a trench in the external ceramic of the thruster SPT-100ML. It was discovered that these microinstabilities develop greatly in the decreasing period of the discharge current and it was also noted that their development makes the drop of the discharge current after its peak value slower, in compare with the increase phase. Frequency of these microinstabilities is on the order of estimated frequency of rotation of electrons in the azimuthal direction in the thruster, what is in coherence with the results of Esipchuk and Tilinin [3]. Obtained results as well as the studies of other scientists gave us more proves of the impact of the microinstabilities on electron transport in Hall thrusters. Therefore we decided to use another, none-intrusive diagnostics to get more precise insight into the problem.

I.2 Experimental setup

To get more local information on microinstabilities, antennas were developed for measurement of electromagnetic field of plasma [10]. These antennas can transmit signals till 20GHz and are capable to resist temperatures ~600°C. They were installed in the external ceramic near the exit of the channel (Fig. 1), the first (A1) with a receiving end parallel to the axis of the thruster, the second (A2) – in the radial direction. The axial position of the antennas was chosen in compliance with the above mentioned criteria of Esipchuk and Tilinin. On azimuth they were separated by 6mm. Correspondingly, A1 is sensitive mostly to the axial electromagnetic field, A2 – mostly to the radial one.

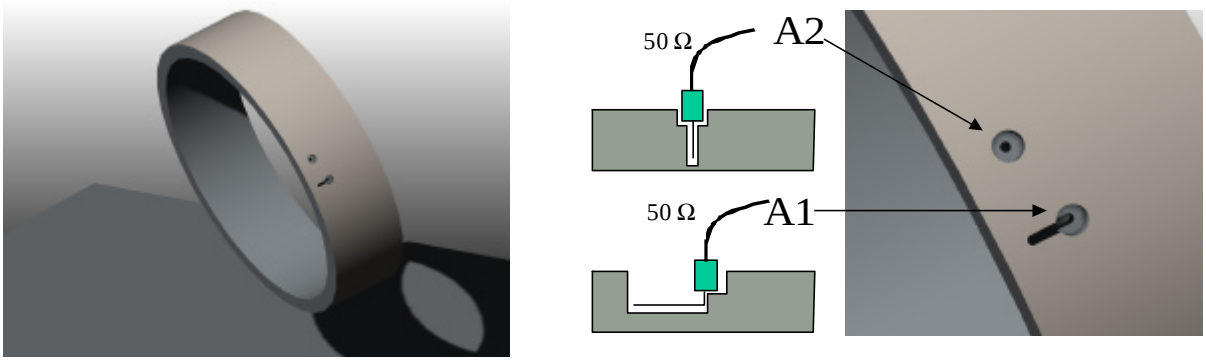

Fig. 1 Scheme of the antennas installation

The antennas were connected to the 50Ω entrance of measurement equipment (oscilloscope, spectrum analyzer) through 50Ω transition lines of the same length. The pass-band of the measurement lines with antennas was tested with use of emitting antenna (excited by HF generator – f<4GHz) which were placed into the discharge channel. The answer of these two lines was constant for signals under 1Ghz, but from 1.5Ghz it is not measurable. One can note that the frequencies of interest (f~5-10MHz) are well in the pass-band of the diagnostics.

Taking into account the thruster geometry, the azimuthal waves should have the length $\lambda=2\pi R/n$, where R is the channel radius, n is integer. It leads to the $k=n/R$ wave number. In our experiments we did not observed instabilities with n>1. It can be attributed to the fact that these instabilities generate an electric field similar to the multipolar one that attenuates like $1/r^n$. The antennas detect only the field radiation on the distances of the

order of the channel width. Therefor, presented here measurements do not allow us to reveal azimuthal microinstabilities having high wave numbers.

I.3 Experimental results

High sampling rate of the oscilloscope ($1 \cdot 10^8$ samp/s) allowed us to obtain A1 and A2 signals sufficiently fine for discovering its structure, and in the same time incorporating more then one period of low frequency discharge current oscillations (Fig. 2) what permitted correlation among these oscillations. During all measurements signal A1 was 5-10 times greater than signal A2. Taking into account that antenna A1 records mostly axial component of the electromagnetic field and A2 – radial one, it is possible to conclude that relatively strong electromagnetic oscillations exist in the axial direction of the thruster. New measurements by the antennas confirm the observation made earlier by the use of the inductive probe [7]. As can be seen in Fig. 2, instabilities detected by the antennas become strong at the decreasing front of the discharge current, whereas near its maximum values at the increasing front they are relatively weak. As HF oscillations in Hall thrusters are related to the electron dynamics this variation of the signals can correlate with electron transport [10]. Expression for electron mobility in Hall thrusters is often considered as composed of several terms from which one (classical) is defined by collisions with heavy particles and another describes an anomalous mobility due to collisions with walls and due to volume turbulence in plasma. Returning to the signals, behavior of the discharge current is well described from the point of view of "predator-pray" fluctuations (see for ex. [4]), related to the fluctuation of neutral number density. Then, in decreasing phase of the discharge current when neutrals are depleting an electron conductivity due to the electron-neutral collisions is decreasing. To sustain current continuity, anomalous conductivity due to plasma turbulence increases what is observed in our case as an increase of antenna signals. In the increasing phase of the discharge current neutrals are filling the channel that leads to an increase of classical electron conductivity and correspondingly to decrease of anomalous conductivity what is observed as decreasing of antenna signals. Of cause, these are purely qualitatively speculations but they are confirmed by other observation which will be shown later.

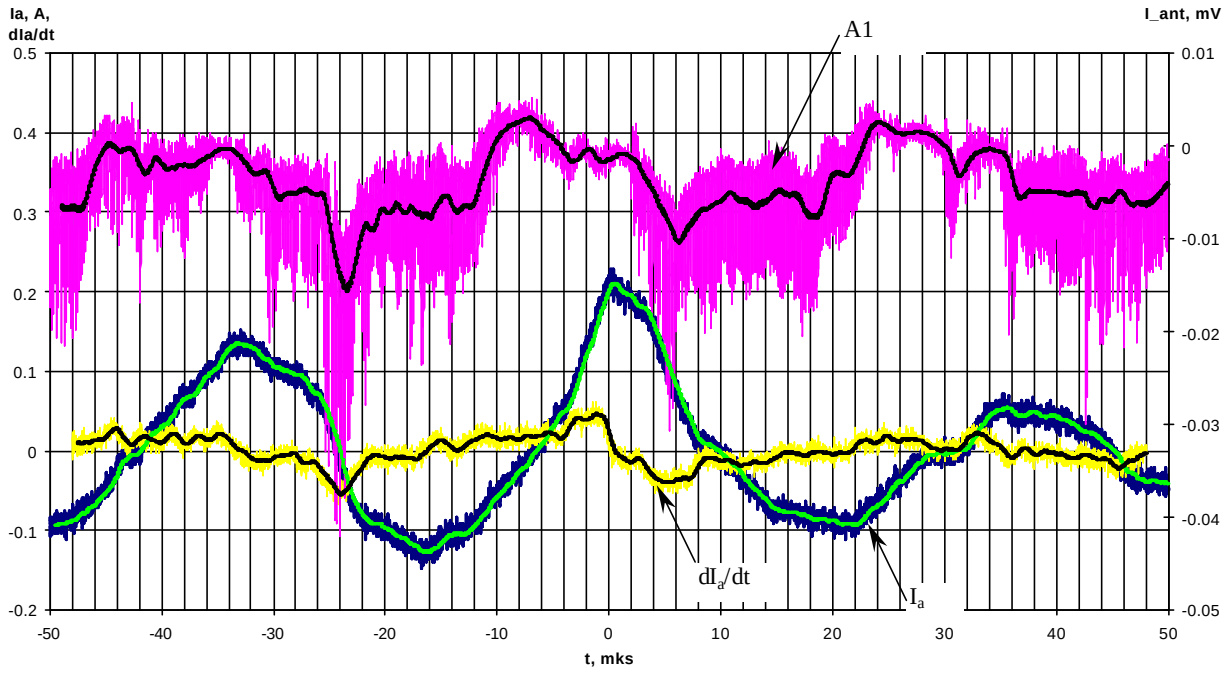

Fig. 2 Examples of AC component (Ia) of the discharge current, Ia derivative and A1 signal

From Fig. 2 one can clearly observe a low frequency modulation of the A1 signal. If one takes a temporal derivative of the registered discharge current then a rather good correlation can be seen between the curve representing averaged A1 signal and the smoothing curve of the derivative (see Fig.2), even taking into account a big error of the numerical differentiation. This result is in a good agreement with Maxwell equations

$$\nabla \times \vec{E} = -m_0 \frac{\partial \vec{H}}{\partial t}, \quad \nabla \times \vec{H} = \vec{J} + e_0 \frac{\partial \vec{E}}{\partial t}$$

from which it is easy to show that variation of current J in time leads to the appearance of electric field E (neglecting $\frac{\partial \vec{E}}{\partial t}$).

Fourier analysis shows that the main frequency of these oscillations is on the order of several MHz [10]. Very large pass-band of the antennas enables the studies of the structure and evolution of A1 and A2 signals, which seem from the first look like a HF noise. Fig. 3 gives a shape of A1 and A2 signals with a very fine resolution of $5 \cdot 10^9$ samp/s. One sees that these signals have a definite form well reproduced both by the antenna A1 and A2. One can see that the signals are in the same phase, but they are not sinusoidal and are slightly shifted in time by $\Delta t \sim 3$-4ns. This shift can not be attributed to the delay in the measurements lines. To cause such a delay, the difference of the lengths of the lines should be on the order of meter whereas in reality it does not exceed several centimeters. Therefore it is possible to come to the conclusion that the antennas register traveling in the azimuthal direction waves. Taking this temporal shift we estimated a wave propagation velocity, which is close to the estimated electron drift velocity, that is:

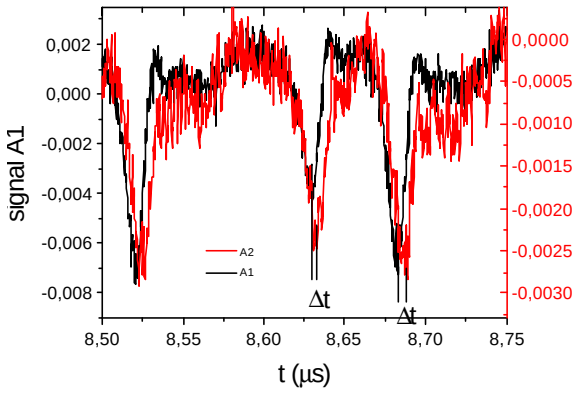

Fig. 3 Evolution of the signals A1 and A2 with sampling rate $5 \cdot 10^9$ samp/s

$$v_q = \frac{d_{antenne}}{\Delta t} = 2.10^6 m/s \approx v_{drift} = \frac{E_z}{B_r} \approx \frac{3.10^4}{150.10^{-4}} \quad (1.1)$$

Moreover, these results are in a good agreement with the results of Esipchuk and Tilinin [1] who observed such waves and identified them as HF azimuthal electron drift waves.

Further analysis of A1 and A2 signals revealed several modes of microinstabilities (Fig. 4). Examples of the prevailing mode are given in Fig.4a and in the left part of Fig.4b. This mode is characterized by the clearly shaped peaks separated by time t_d comparable to the time of one tour of electron cloud rotating with drift velocity in the azimuthal direction. Indeed, assuming length of the rotation $L=2\pi R_{ext}=2\pi \cdot 0.05 \approx 0.314$ m and taking time interval between the peaks $t_d=0.15$mks we get a velocity $2.1 \cdot 10^6$ m/s, that is in an excellent agreement with the averaged electron drift velocity (see eq.1.1). Based on this observation we classified another modes of the signals. Fig.4c presents a case where between two peaks separated by t_d there is another well-shaped peak. Fig.4d presents a case where we observed in-between two peaks. It necessary to note that all these conclusions concern the parts of the signals with a sufficiently large amplitude. Signals from the 24-30mks range (see Fig.2), for example, are very weak and it is impossible to obtain any structure. Transition to such a range is shown in Fig.4b.

This strong correlation between the time t_d of signals peaks separation and the time of one tour of electron cloud rotating with drift velocity gave us an idea for this phenomena explanation. We suggest that these peaks are due to the fluctuations of electron number density which appear in the random positions and rotate in the azimuthal direction with the velocity of electron drift [10]. In certain moments there appear several such fluctuations, as in the case of Fig.4c,d (peaks supposed to originate from the same fluctuation and separated by the time $\sim t_d$ are marked), these fluctuations rotate with slightly different velocities and eventually merge into one. A middle-width of the peaks can then give an estimation of the azimuthal dimension of such a fluctuation. Taking the value of 10ns we come to length of ~2 cm.

A close look at the A1 and A2 signals shows a sliding of period between the “main” peaks during the acquisition – from values ~12mks to ~18mks (when these peaks are clearly distinguished), and this variation of the period has a strong correlation with discharge current low-frequency oscillations (Fig.5). The period between “main” peaks reaches the lowest values near the discharge current minimum, at the decreasing front. We suppose that such a variation gives an estimation of the total axial electric field variation in the accelerating channel. Indeed, an azimuthal velocity of the fluctuation propagation is close to the electron drift one and given by eq. (1.1). Assuming a constant magnetic field, a lower value of the period of these peaks means a higher propagation velocity and therefore a higher axial electric field. That is, a higher axial electric field appears at the decreasing front of the discharge current near its minimum. Increasing of the axial electric field during the phase of decrease of discharge current is understandable from the point of view of electron transport: above mentioned depletion of neutrals during this phase leads to the lower electron conductivity and electric field tries to compensate it. The relative oscillation of the period between peaks

gives the relative amplitude of electric field oscillations which means that according to our observations electric field can change ~±20% relatively its middle value. It is in a good agreement with the results of numerical simulation represented in part 2 of the paper. At the same time, an increasing of the axial electric field is probably not the only mechanism responsible for enhancement of electron conductivity to anode.

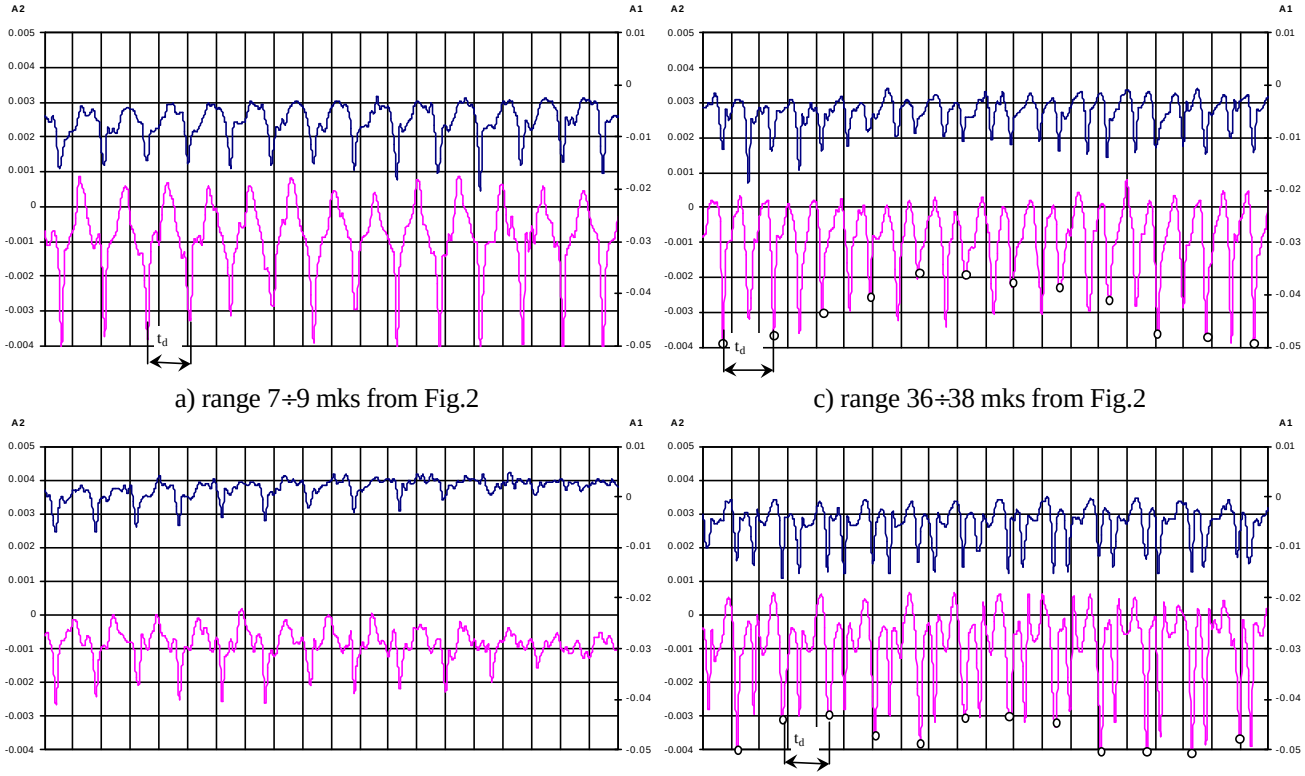

a) range 7÷9 mks from Fig.2

c) range 36÷38 mks from Fig.2

b) range 22÷24 mks from Fig.2

d) range 40÷42 mks from Fig.2

Fig. 4 Different modes of A1 and A2 signals during acquisition

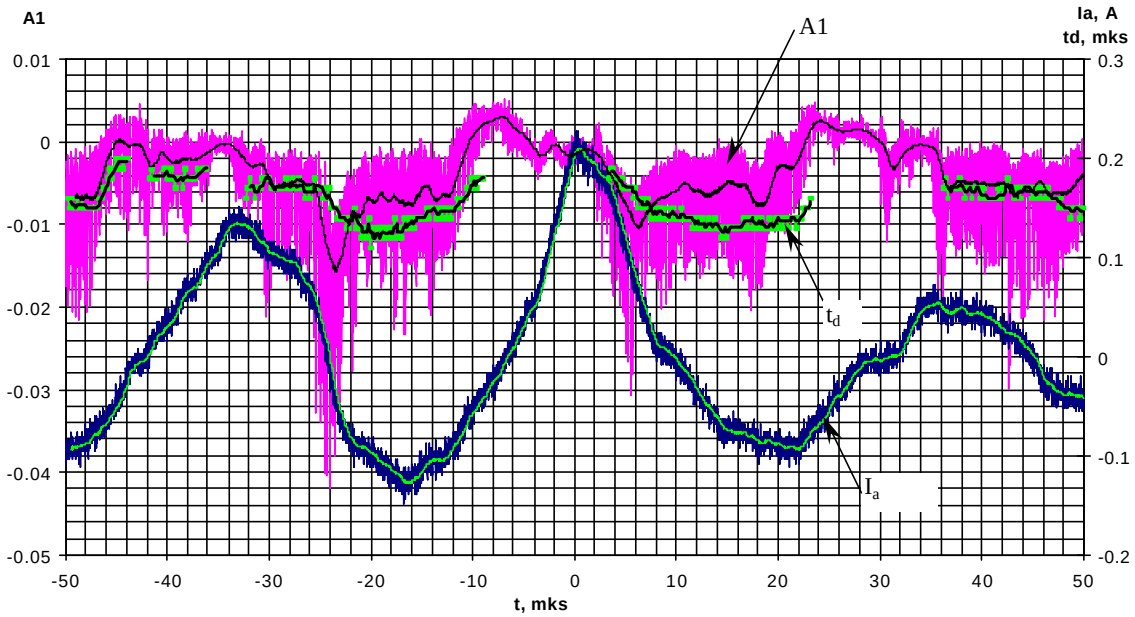

Fig. 5 Variation of the A1 signal, discharge current alternating component (Ia) and period between peaks of the A1 signal (t_d)

II. PIC MCC Model

In order to study the stability of the plasma in the direction of rotation due to the ExB drift we have developed a fully kinetic bidimensional model of the Hall thruster. To this purpose the geometry that we have retained is the following. The simulation box is a rectangle with periodic boundaries in one direction. In

the other direction the boundaries are open and a given voltage is applied. This direction is parallel to the channel axis, it will be called x in all the following. The other direction will be called y, it models the azimutal direction. Thus the rectangle models a cylinder of an arbitrary radius inside the thruster that would have been opened along one of it generatrix. A magnetic field perpendicular to the plane is also applied. It is uniform in the y direction and presents a spatial dependence along the x direction. This field models the radial component of the magnetic field of the Hall thruster. The Xenon is handled through fluid equations. Electrons collisions with the Xenon are taken into account as well as self consistent ionization. For this purpose the velocity space is 3 dimensional. In order to get read of the highest frequencies corresponding to the electron plasma frequency the model is implicit for electrons and explicit for ions . Unfortunately one must resolve the electron cyclotron frequency as well as the larmor radius which means time scale of the order of 10^{-9} s while at the same time one has to follow the time evolution of the system for few hundred of microseconds in order to observe the evolution of the Xenon. This means typically 10^6 times steps ,which make the simulations extremely time consuming. In order to alleviate somewhat this cost we have reduce the periodicity length to only one sector of variable angle of the cylinder. This reduces the number of points in the transverse direction. We have checked for various conditions that this does not affect the results.

II.1 Numerical algorithms

In the following section we describe more precisely the algorithms that are used.
The discretized equations of motion for the ions are integrated using a classic explicit leap-frog scheme with a force only due to the electric field thus the new velocity and position are given by the relationship :

$$\begin{aligned} \mathbf{v}^{n+1/2} &= \mathbf{v}^{n-1/2} + \Delta t \frac{e}{m_i}\mathbf{E}^n \\ \mathbf{x}^{n+1} &= \mathbf{x}^{n-1} + \Delta t\, \mathbf{v}^{n+1/2} \end{aligned} \tag{2.1}$$

The discretized equations of motions for the electrons are integrated using an implicit scheme.

$$\mathbf{x}^{n+1} = \mathbf{x}^n + \Delta t\, \mathbf{v}^{n+1/2}, \tag{2.2a}$$

$$\mathbf{v}^{n+1/2} = \mathbf{v}^{n-1/2} + \Delta t\, \bar{\mathbf{a}}^n - \Delta t\left(\frac{\mathbf{v}^{n+1/2}+\mathbf{v}^{n-1/2}}{2} \right) \times \frac{e\mathbf{B}(\mathbf{x}^n)}{m_e c}, \tag{2.2b}$$

where $\bar{\mathbf{a}}^n = \frac{1}{2}\left(\bar{\mathbf{a}}^{n-1} - \frac{e}{m_e}\mathbf{E}^{n+1}\left(\mathbf{x}^{n+1}\right) \right)$.
The implicit method which has been chosen is the so-called direct one that uses a predictor-corrector scheme to uncouple the equations of evolution of the electrons and the equations of the fields.
The equations corresponding to the predictor step can be written as :

$$\begin{aligned} \tilde{\mathbf{v}}^{n+1/2} &= \mathbf{v}^{n-1/2} + \frac{\Delta t\, \bar{\mathbf{a}}^{n-1}}{2} - \Delta t\left(\frac{\tilde{\mathbf{v}}^{n+1/2} + \mathbf{v}^{n-1/2}}{2} \right) \times \frac{e\mathbf{B}(\mathbf{x}^n)}{m_e c} \\ \tilde{\mathbf{x}}^{n+1} &= \mathbf{x}^n + \Delta t \tilde{\mathbf{v}}^{n+1/2} \end{aligned} \tag{2.3}$$

These equations only use quantities known at previous times as in an explicit scheme. From the predicted position at time level n+1 one can then compute a predicted charge density $\tilde{\rho}_e^{n+1}$.
The true electron charge density is then extrapolated from the predictor step and is written as :

$$\rho_e^{n+1} = \tilde{\rho}_e^{n+1} + \delta\rho_e \tag{2.4}$$

$\delta\rho_e$ is then computed by expressing $\delta\mathbf{x} = \mathbf{x}^{n+1} - \tilde{\mathbf{x}}^{n+1}$ as a function of the electric field at time t^{n+1}. Poisson equation then writes :

$$\mathrm{div}\left(\mathrm{I} + \chi_e\right).\mathbf{E}^{n+1} = \frac{\rho_i^{n+1} - \tilde{\rho}_e^{n+1}}{\varepsilon_0} \tag{2.5}$$

where $\chi_e(x, y)$ is a tensor defined as $\chi_e = \frac{\Delta t^2}{4\varepsilon_0}\tilde{\rho}^{n+1}\left(\mathrm{I} + \mathrm{R}\right)$
In the preceding expression I is the identity matrix while R is the rotation matrix that dependent on the magnetic field structure. In our particular geometry it writes :

$$R(x,y) = \frac{1}{1+\frac{\Delta t^2 B_z^2}{4}} \begin{pmatrix} 1-\frac{\Delta t^2 B_z^2}{4} & -\Delta t B_z \\ \Delta t B_z & 1-\frac{\Delta t^2 B_z^2}{4} \end{pmatrix}$$

B_z is the imposed magnetic field in the radial direction. Finally, the corrector step for the electrons motion is:

$$\begin{aligned} \delta\mathbf{v} &= -\frac{e\Delta t}{2m_e}\left[\mathbf{E}^{n+1}(\tilde{\mathbf{x}}^{n+1}) + \delta\mathbf{v}\times\mathbf{B}(\mathbf{x}^n)\right] \\ \mathbf{x}^{n+1} &= \tilde{\mathbf{x}}^{n+1} + \Delta t\,\delta\mathbf{v} \\ \mathbf{v}^{n+1/2} &= \tilde{\mathbf{v}}^{n+1/2} + \delta\mathbf{v} \end{aligned} \qquad (2.6)$$

II.2 Electron-wall collisions

As mentioned above, the model is two dimensional (in the axial direction and azimutal direction) but the velocity space has three dimensions. The time of flight of particles in the transverse direction is computed. This allows to take collisions with the walls and the effect of the Debye Sheath into account. The Debye sheath is considered as a discontinuity (infinitely thin sheath) in the potential and the Debye sheath voltage is not calculated self-consistently. Electrons reaching the wall with radial energy larger than the assumed Debye sheath potential are isotropically reflected by the wall while electrons with radial energy below the sheath potential are specularly reflected by the sheath. The value of the sheath potential taken in the calculations was 20 eV which in effect eliminates most of the electron-wall collisions.

II.3 Electron-atom collisions

The neutral transport is described with a one dimensional fluid model. The corresponding equation are :

$$\frac{dn_a}{dt} + \frac{d(n_a v_{ax})}{dx} = -\nu_{ionize} n_a \qquad (2.7)$$

$$\frac{dn_a v_{ax}}{dt} \frac{d(n_a v_{ax}^2 + 2n_a D_{xx})}{dx} = -\nu_{ionize} n_a v_{ax} \ , \quad D_{xx} \approx \frac{kT}{6m_a} \qquad (2.8)$$

In these equations n_a is the xenon atoms density, v_{ax} is the xenon velocity, and D_{xx} is an average energy dispersion which value has been obtained as a fit to the results of a Monte Carlo study of the xenon flow. These equations assume a specular reflection of the atoms of xenon on the wall. A more sophisticated model has been developed but the simplified model is sufficient for our purpose.
A simplified set of cross-sections has been used for electron-xenon collisions. It includes momentum transfer and ionization cross-sections. Other inelastic collisions are neglected and collisions with excited xenon atoms are not included. The coupling of the xenon fluid equations with the particles is done in the following way. At a given time knowing the Xenon density (assumed homogeneous in the transverse direction) and the local electron density one compute the probability of ionization of the xenon by a given electrons. If the probability is acceptable a new ion and electrons at rest are created in the cell where the electron is located. The total number of atoms ionized is then averaged in the transverse direction to compute the average density of atoms that have been ionized during this time step. This gives directly the term $\nu_{ionize} n_a$ of the RHS of the fluid equations that are then advanced of one time step

II.4 Results of simulation and discussion

The following input parameters were chosen for the numerical simulation:

Calculation region length	3 cm
Channel length	2.5 cm
Inner radius	2 cm
Outer radius	4 cm
Gas	xenon
Flow rate of the gas	2.5mg/s
Temperature of the gas at the anode	640°C
Applied voltage	300 V
Magnetic field at exhaust	200Gauss

The profile of the magnetic field used in the simulation is shown in Figure 6. The field has a maximum at the exit of the thruster and wall collisions are set to zero between 2.5 and 3 cm which correspond to the absence of walls outside of the thruster. Figure 7 shows the time dependence of the ionic and electronic currents on the cathode side, positive values correspond to the ion current, negative values to electron. The average value of electronic current is approximately 30% of the ionic one. The frequency of oscillation is in the range of 20kHz. The current intensity and the frequency of oscillations are in reasonable agreement with experimental results. Figure 8 shows the ratio of the ionic current to the total current measured again at the cathode. The spatio temporal evolution of the Xenon density expressed as the number of particles per cubic meter is displayed in Figure 9. Relaxation oscillations due to ionization with the same frequency as the current oscillation are clearly visible. The average value at the exit oscillates between 10^{17} and 10^{18} particules/m^3 which is far too low to explain the observed current. We have used a Debye sheath of 20 eV and the injection temperature of electrons was 1eV. For these parameters wall collisions are also too small to explain the conductivity. This means that it can only be explain by a turbulent mechanism. The existence of a large turbulent field is clearly visible in Figure 10. The solid curve shows the average value of the electric field along the channel which peaks about $5 \cdot 10^4$V/m approximately 0.5cm inside the thruster and as a dotted curve represents the average value of the square of the fluctuations of the electric field in the transverse direction. The maximum value is close to the exit of the thruster and it peaks to the rather large value of 10^4V/m which represents 20% of the accelerating field. A full picture of the spatial structure of the transverse electric field is shown in Figure 11. One can see that the amplitude of the fluctuations of this field is od the order of 5 10^4V/m.

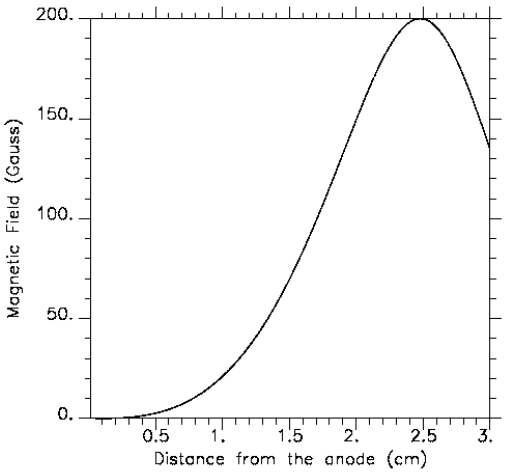

Fig. 6 Profile of the magnetic field used for the simulation

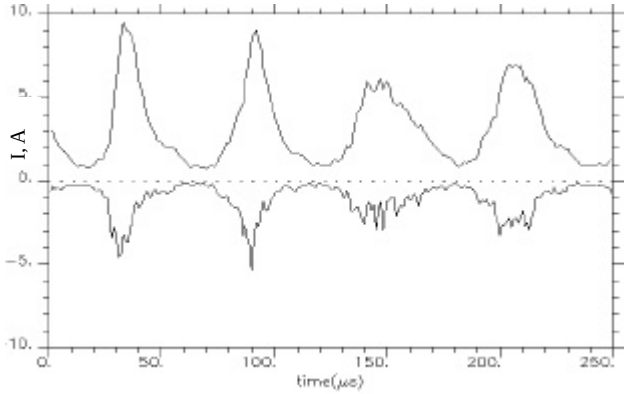

Fig. 7 Ion and electron current in the cathode zone

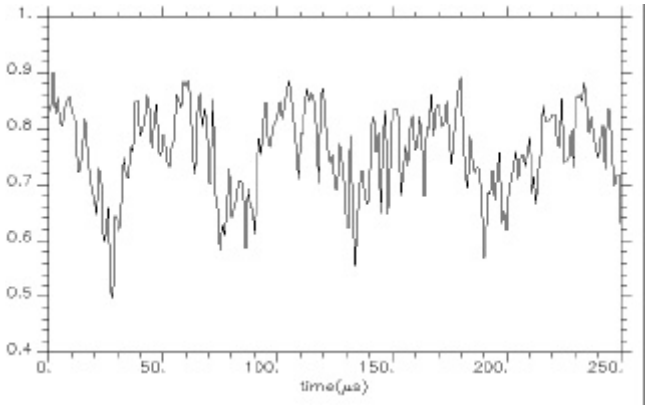

Fig. 8 Ratio of the ion current to the total in the cathode zone

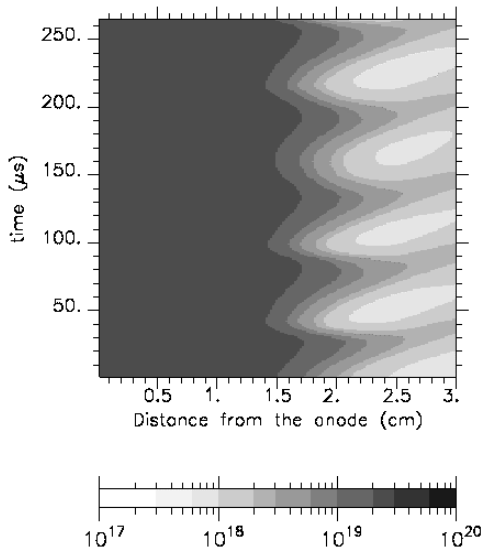

Fig. 9 Spatio-temporal evolution of the Xe density

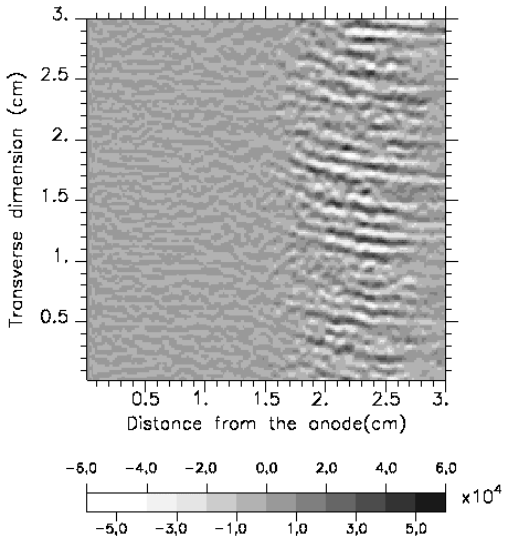

Fig. 11 Spatial structure of the transverse electric field

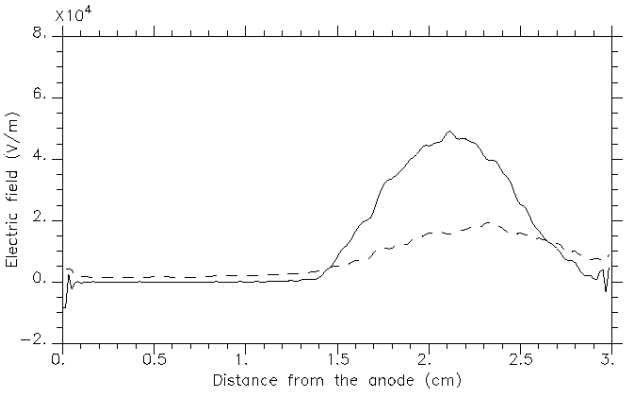

Fig. 10 Distribution of the electric field and of square of its fluctuation in the axial direction

III. Derivation and study of the dispersion relation of a magnetized beam

As seen in Fig.12, the simulation shows that electrons are drifting across the magnetic field with a velocity spread. This velocity dispersion amplitude is comparable to the drift velocity and is generated by the turbulence itself or by the electron heating in the stationary electric field. In order to understand the origin of this turbulence, we have studied the dispersion equation of electrostatic waves in a hot magnetized electron beam drifting across a magnetic field with non magnetized cold ions. Such waves have already been considered by many authors ([11] and references quoted there), but they usually restrict the analysis to cases where the drift velocity V_D is much smaller than the electron thermal velocity. In order to find an instability with frequency lower than the electron cyclotron frequency, these authors have to take into account gradients or a small wave number component along the magnetic field. Here, we consider cases where V_D is not small with respect to the electron thermal velocity. Consequently, we assume that the stationary electric field drift velocity V_D is much larger than the magnetic field gradient drift velocity and than the density gradient drift velocity which will both be neglected. This corresponds to the conditions where the turbulence is observed in the simulation.

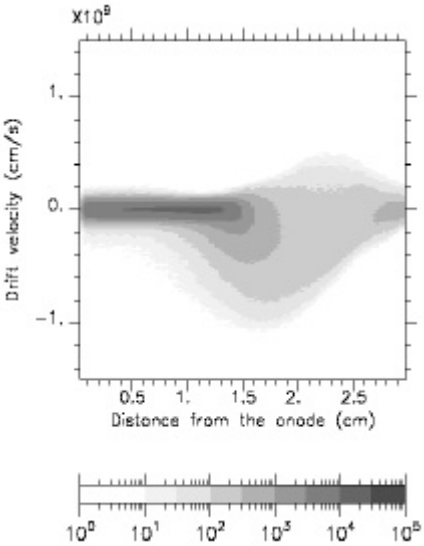

Fig. 12 Variation of electron drift velocity (simulation results)

Assuming electrostatic field perturbations $\phi = \phi_0 \exp(-i\omega t + k)$ and a maxwellian electron distribution function with a velocity shift V_D and temperature T, the dispersion equation can be written:

$$k^2\lambda_D^2(1-\frac{\omega_{pi}^2}{\omega^2}) = I_0(b)e^{-b} - 1 + \sum_{n=1}^{n=\infty} I_n(b)e^{-b}\frac{2(\omega - kV_D)^2}{(\omega - kV_D)^2 - n^2\Omega^2} \tag{3.1}$$

where $\lambda_D^2 = T/m\omega_{pe}^2$, $b = k^2T/m\Omega^2$, m being the electron mass, $\omega_{pe,i}$ the electron or ion plasma frequencies and Ω the electron cyclotron frequency. The functions I_n are modified Bessel functions of order n. For b<<1, the dispersion equation reduces to:

$$(1 - \frac{\omega_{pi}^2}{\omega^2}) = \frac{\omega_{pe}^2}{(\omega - kV_D)^2 - \Omega^2} \tag{3.2}$$

which has no unstable solution in the relevant domain of parameters. Assuming now $\omega << k V_D$ without restriction on b, unstable roots appear whenever $F(k,V_D)>0$ where

$$F(k,V_D) = I_0(b)e^{-b} - 1 + \sum_{n=1}^{n=\infty} I_n(b)e^{-b}\frac{2(kV_D)^2}{(kV_D)^2 - n^2\Omega^2} - k^2\lambda_D^2 \tag{3.3}$$

It is seen that transitions from stability to instability occur when kV_D is close to $n\Omega$. Setting $kV_D = n_0\Omega + \delta$ with $\delta << \Omega$, the wave is unstable for $\delta > 0$ with a growth rate:

$$\gamma = k\lambda_d\omega_{pi}\left(\frac{\delta}{n_0\Omega}I_0e^{-b}\right)^{1/2} \tag{3.4}$$

Another transition from instability to stability has to take place between $kV_D = n_0\Omega$ and $kV_D = (n_0+1)\Omega$ for values of k in the vicinity of k_0 with $F(k_0)=0$. For k slightly smaller than k_0, the growth rate peaks sharply reach:

$$\gamma \approx \sqrt{\frac{3}{2}}(k_0\lambda_D)^{2/3}\left(\frac{k_0V_D\omega_{pi}^2}{\left|V_D\frac{\partial F}{\partial V_D}\right|}\right)^{1/3} \tag{3.5}$$

These results are displayed on the next figures which show numerical solutions of the full dispersion equation (3.1), where V_T – thermal electron velocity.

Figure 13 represents the real part ω of the solution as a function of V_T/V_D and of kV_D. The parameters chosen corresponds to the ones measures in the simulations. Frequencies are given in Hertz. Values of ω of the order of 10^7 up to 10^8 are visible at the edges of the unstable regions. This corresponds to frequencies ranging form 1Mhz to 10Mhz. The spectral analysis of the modes observed in the simulations gives frequencies between 1 and 3Mhz which agrees with the preceding range of frequencies. The absence of the highest frequencies is probably due to the cut-off introduced by the implicit scheme.

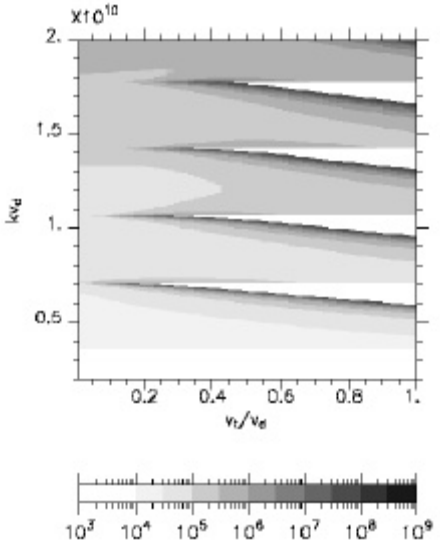

Fig. 13 Real part of the numerical solution of the full dispersion equation

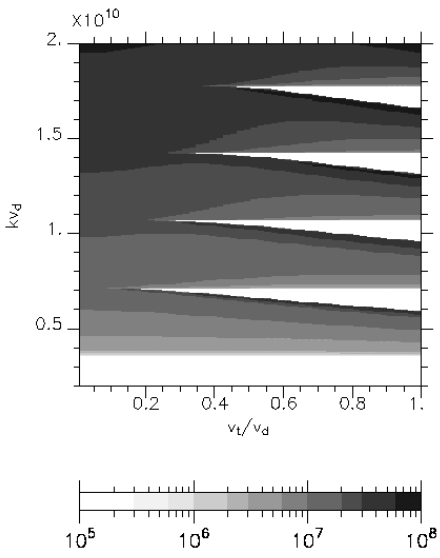

Fig. 14 Imaginary part of the numerical solution of the full dispersion relation

Figure 14 represents the imaginary part γ of the solution in the same parameters space. Large values of the order of 10^7 up to 10^8 can be observed. This corresponds to growth time ranging from

0.1μs down to 0.01μs which are very short times indicating a very unstable situations. Of course with such large growth rate the linear phase of the instability cannot be observed in the simulation and the perturbation that we observe corresponds to the saturated state of the instability.

Conclusions

Presented results reveal a direct correlation of the microinstabilities from the frequency band 1-10MHz in the accelerating channel and macroscopic characteristics of Hall-effect thrusters. Experimental results were obtained by the use of two HF antennas installed in the external wall of the accelerating channel and shifted in the azimuthal direction. Experiments show existence of significant HF oscillations in the axial direction of the thruster which are related to the variation of axial electric field induced by the axial current. This oscillations reach the highest amplitude at the decreasing front of the discharge current which was supposed to be related to the changes of electron conductivity. Observed temporal shift of signals from two azimuthally separated antennas and the similarity of their forms allowed for conclusion that this is an azimuthally propagating wave with the velocity close to the electron drift one. This conclusion is in agreement with observations of other authors [1]. Closer look at the HF signals revealed their definite structure. We suggest that the source of this signal is fluctuations of electron number density rotating in the azimuthal direction with the velocity of electron drift. On the base of this assumption it was shown a close relation of these HF oscillations with axial electric field. Also was shown that variation of the axial electric field can reach ~20%.

For the study of stability of the plasma in the azimuthal direction there was developed a fully kinetic 2D model of a Hall thruster. There was show an existence of a large turbulent axial electric field which is responsible for the observed electron conductivity in this direction. Amplitudes of this field are in good agreement with that ones reduced from the experiments.

Studying of the dispersion equation for electrostatic waves in plasma showed existence of HF instabilities in the frequency range 1-10MHz with very short growth times.

In the future work it is planned a more thorough study of microinstabilities with larger number of the antennas suitably placed in the ceramic of the thruster. The new enhancements into the numerical code will allow to characterize more precisely phenomena related to electron dynamics.

This work has been performed in the frame of the research group GDR n°2232 CNRS/CNES/SNECMA/ONERA "Propulsion à Plasma pour Systèmes Spatiaux".

References

[1] Esipchuk Yu.V. and Tilinin G.N. Zh. Tekh. Fiz. 46, pp. 718-729, 1976 (Sov. Phys. Tech. Phys. 21, 417, 1976)
[2] Morozov A.I. et al.; Zh. Tekh. Fiz. 42, pp. 612-619, 1972 (Sov. Phys. Tech. Phys. 17, 482, 1972)
[3] Esipchuk Yu.V. et al Zh. Tekh. Fiz. 43, pp. 1466-1473, 1973 (Sov. Phys. Tech. Phys. 18, 928, 1974)
[4] E.Y. Choueiri Characterization of oscillations in closed drift thrusters AIAA-94-3013, 30th Joint Propulsion Conference, IN, USA, 1994
[5] Bouchoule A., Philippe-Kadlec C., Prioul M., Darnon F., Lyszyk M., Magne L., Pagnon D., Poche S., Touzeau M., Bechu S., Lasgorceix P., Sadeghi N., Dorval N., Marque J.P., Bonnet J. “Transient phenomena in closed electron drift plasma thrusters: insights obtained in a French cooperative program”, Plasma Sources Science and Technology, May 2001, 10(2), 364-377.
[6] Morozov A.I., Savelyev V.V. “Fundamentals of Stationary Plasma Thruster Theory”, Reviews of Plasma Physics, 21.
[7] M.Prioul, A.Bouchoule, S.Roche, L.Magne, D.Pagnon, M.Touzeau, P.Lasgorceix “Insights on Physics of Hall Thrusters through Fast Current Interruptions and Discharge Transients” – IEPC-01-059, 27th International Electric Propulsion Conference, Pasadena, USA, 2001
[8] Heron A., Adam J.C. Internal report DTS/AE/MTE/3P-01 235, 2001.
[9] Morozov A.I., Neverovsky V.A., Smirnov V.A. Zh. Tekh. Fiz. 43, pp. 535-542, 1973.
[10] M.Prioul “Experimental study of Hall-type thrusters”, PhD thesis, Orleans University, France, 2002.
[11] N.A.Krall and F.C.Liewer, Phys. Rev.A, **4**, 2094, 1971